

An Enhanced Oscillator Model for Clock Synchronization Protocols

Balázs Renczes, Tamás Kovács házy
 Department of Measurement and Information Systems
 Budapest University of Technology and Economics
 Budapest, Hungary
 renczes@mit.bme.hu, khazy@mit.bme.hu

Abstract— This paper describes an enhanced oscillator model that is able to handle several disturbing noise sources influencing its instantaneous frequency and/or phase. Besides the well-known white and random walk frequency noises, also flicker noise is generated. It is highlighted that flicker noise can only be applied with limitations. Furthermore, the model is able to accept the temperature dependence of the oscillator as input. Although this is an important influencing parameter, especially for low-cost oscillators, this effect is often neglected. Therefore, with this supplement, a more realistic oscillator model can be achieved. The functionality of the model is demonstrated through simulations. During the tests, three temperature patterns along with generally assumed Gaussian type noise sources are investigated in order to simulate real circumstances. The effects are analyzed by help of Allan variance plots. It is highlighted that for long time intervals, temperature dependence affects the Allan variance of low-cost and temperature compensated crystal oscillators (TCXOs) considerably.

Keywords—oscillator model, clock synchronization, white frequency noise, flicker noise, random walk noise, Allan variance, TCXO

I. INTRODUCTION

With the expansion of distributed signal processing, the importance of precise clock synchronization has become of major importance. It is applied, among others, in large industrial network systems [1], computer numerical control systems [2] and smart grids [3]. IEEE Standard 1588-2008 has been published in order to describe the details of precision time protocol (PTP). Its importance can be illustrated by the fact that a separate standard has been published in order to determine the utilization of PTP in power system applications [4].

The PTP protocol assumes that the oscillators of the local clocks are inaccurate, compared to that of the master clock, to which the local clocks should be synchronized. Oscillator errors are in order of magnitude of *ppm* (part per million, 10^{-6}), for precision oscillators even of *ppb* (part per billion, 10^{-9}). In order to keep the overhead in network traffic low, the synchronization interval is in the order of magnitude of 1/16–1 second. At the instant of synchronization, the frequency and the offset error of the clock is compensated. These error sources will be described in detail in Section II. Once the synchronization is performed, the oscillator is running free until the next synchronization. Since the synchronization interval is significantly larger than the cycle time of the local oscillators, it is important to keep errors at the instant of synchronization as low as possible. This is achieved by the clock servo.

For the description of this control mechanism, several papers have been published. In the clock servos, mostly, but not exclusively, a proportional-integral (PI) or a proportional-integral-derivative (PID) controller is applied to control the local oscillator. In [6], a PI-controller is applied to fine-tune the frequency of the local oscillator, while in [7], the performance of a two-state Kalman filter is analyzed in detail, assuming that the local oscillator frequency is distorted by white noise and random walk noise. In [8], a clock servo is designed with applying both a Kalman filter and a PID controller, and it is shown that on large time scales, this servo outperforms the method based on PI-controllers. The effect of quantization errors can also be taken into consideration. To this aim, in [9], a feedforward filtering technique is applied, while in [10], Kalman filtering along with a PI-controller is utilized.

Before realizing the above-mentioned techniques, it is advantageous, if their behavior can be simulated. To this aim, it is crucial that local oscillators can be modeled. This paper is intended to give this model, taking different noise sources into consideration.

The paper is organized as follows: in Section II, the clock model will be introduced, describing an ideal clock and noise sources. Furthermore, the Allan variance, as a general evaluation technique will be described. In Section III, different noise sources will be generated, highlighting some issues that should be handled, and introducing some common temperature patterns. In Section IV, the effect of these noise sources will be highlighted, with a special emphasis on temperature dependence. Finally, Section V concludes the paper.

II. CLOCK MODELS FROM IDEAL TO REALISTIC

A. General clock model

An ideal clock can be described by a sinusoidal oscillator. The output function of the oscillator is a periodic signal:

$$v(t) = V_0 \cdot \cos(2\pi f_0 t + \Phi_0) , \quad (1)$$

where V_0 is the amplitude of the signal, while f_0 and Φ_0 denote the frequency and the phase of the signal at $t = 0$, respectively. The cycle time of this ideal oscillator is $1/f_0$. In a real clock, several noise sources distort this cycle time. A general description of a real clock can be given as

$$v(t) = V_0 \cdot \cos(2\pi f_0 t + \Phi(t)) , \quad (2)$$

that is, the noise sources are modeled in the time dependence of $\Phi(t)$. In order to characterize these errors, [11] defines the following quantities:

$$\vartheta(t) = \frac{f(t) - f_0(t)}{f_0}, \quad (3)$$

which is the normalized frequency deviation of f from the nominal value. Applying this value, the time deviation is defined as

$$x(t) = \int_0^t \vartheta(t^*) dt^*. \quad (4)$$

and expressed with phase error it equals to

$$x(t) = \frac{\Phi(t)}{2\pi f_0}. \quad (5)$$

B. Noise sources

The errors of the oscillator can be characterized either in the time or in the frequency domain [12]. In [13], it has been shown that the noise sources can be separated in the frequency domain, based on the derivatives of the power law spectrum. In other words, they can be separated based on powers, to which the power law spectrum is proportional to. In [11], the power law spectra of ϑ , that is, $S_\vartheta(f)$ are applied, and it is pointed out that these spectra are proportional to f^α .

In the time domain, the errors can be characterized based on the measurement/simulation samples of the phase error. Let us denote the k^{th} sample of the phase error by x_k . With this notation, an on average frequency error can be determined between two samples:

$$\bar{\vartheta}_k^{\tau_0} = \frac{x_{k+1} - x_k}{\tau_0}. \quad (6)$$

where τ_0 denotes the time interval between the samples [11]. With this definition, the Allan variance can be defined as:

$$\sigma_\vartheta^2(\tau) = \frac{1}{2} E\{(\Delta \bar{\vartheta}^\tau)^2\} \quad (7)$$

where $E\{\cdot\}$ denotes the expected value operator [12]. With a finite sample set of N elements, it can be approximated as

$$\sigma_\vartheta^2(\tau) \approx \frac{1}{2 \cdot (M - 2n + 1)} \cdot \sum_{k=1}^{M-2n+1} (\bar{\vartheta}_{k+n}^\tau - \bar{\vartheta}_k^\tau)^2 \quad (8)$$

where $\tau = n\tau_0$ [11]. An alternative description is

$$\sigma_\vartheta^2(\tau) \approx \frac{1}{2\tau^2 \cdot (M - 2n + 1)} \cdot \sum_{k=1}^{M-2n+1} (x_{i+2n} - 2x_{i+n} + x_i)^2 \quad (9)$$

In the Allan variance plots, different noises are proportional to different powers of τ , that is, $\sigma_\vartheta^2(\tau) \sim \tau^\mu$. Noise sources, along with their α and μ values are contained in Table I.

TABLE I. NOISE SOURCES AND THEIR CHARACTERISTIC VALUES [11]

Noise type	α	μ
random walk frequency noise	-2	1
flicker frequency noise	-1	0
white frequency noise	0	-1
flicker phase noise	1	-2
white phase noise	2	-3

Besides these effects, the temperature dependence of the oscillators will also be investigated. This dependence can be avoided if the temperature of the oscillator is kept constant, as it is performed at oven-controlled crystal oscillators (OCXOs). However, the cost of such oscillators is rather high. For temperature-compensated crystal oscillators (TCXOs), the temperature is not kept constant. However, the frequency of the oscillator is compensated over a wide temperature range. As this compensation is not perfect, temperature dependence occurs. This also holds for low-cost oscillators, where no such compensation is performed. Models of temperature dependence can also be created for these oscillators.

III. GENERATION OF NOISE SOURCES

In this Section, the method of noise source generation will be highlighted. It will be shown that the generation of white and random walk noise sources is quite straightforward. Contrarily, it will be shown that flicker noise can only be generated approximately. Finally, some characteristic temperature profiles will be presented.

A. White and random walk noise sources

White noise can be easily generated, as a sequence of zero-mean numbers of Gaussian distribution, with a given standard deviation. Let us assume we have generated a series of white frequency noise, and let us denote the k^{th} sample with $n_{WF,k}$. Each sample in the sample set has the same distribution, that is, a normal distribution with zero-mean and standard deviation σ_{WF} :

$$n_{WF,k} \sim N(0, \sigma_{WF}). \quad (10)$$

From a white normally distributed zero-mean white sample set, a random walk frequency noise can be generated by the following equation:

$$n_{RW,k} = \sum_{i=1}^k n_{WF^*,i}, \quad (11)$$

where $n_{RW,k}$ is the k^{th} sample of the random walk noise. Notation n_{WF^*} has been introduced in order to highlight the difference between white frequency noise as a noise source in (10) and white frequency noise that generates the random walk

noise. The distribution of $n_{RW,k}$ is also normal, with the following distribution:

$$n_{RW,k} \sim N(0, \sqrt{k} \cdot \sigma_{WF^*}). \quad (12)$$

White phase noise can be generated in the same way, as white frequency noise. The only difference is that it influences values x_k instead of ϑ_k .

B. Flicker noise

Contrarily to the white noise and random walk noise sources, flicker noise cannot be generated easily. The power law spectrum of a flicker frequency noise has an α value of -1 , see Table I. It means that it is inversely proportional to the frequency. This noise source can be generated, if a white frequency noise, which has a constant power law spectrum, is filtered [14]. More specifically, the filter should have a transfer function proportional to $1/\sqrt{f}$. This kind of filter cannot be realized perfectly. However, it can be approximated by an infinite impulse response (IIR) filter with the following transfer function [15]:

$$H(z) = 0.01 \cdot \frac{4.99 - 9.60z^{-1} + 5.06z^{-2} - 0.44z^{-3}}{1 - 2.49z^{-1} + 2.02z^{-2} - 0.52z^{-3}}. \quad (13)$$

Let us investigate the effect of this filtering. The input of the filter is white noise, with zero-mean, and standard distribution of $\sigma_{WF^{**}} = 10^{-8}$ s. The power spectrum of this frequency noise, assuming sampling frequency $f_s = 10$ Hz is depicted in Fig. 1.

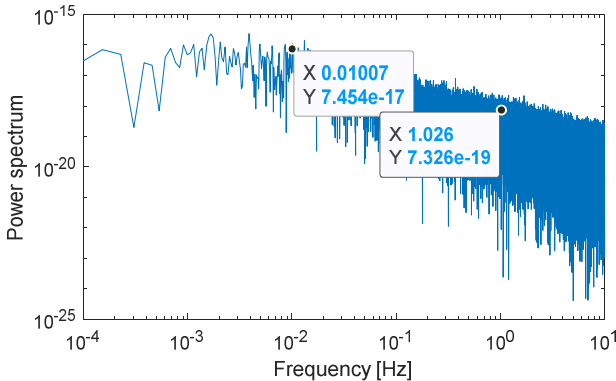


Fig. 1. Power spectrum of the generated flicker frequency noise

As expected, according to Table I, at higher frequencies, the spectrum is inversely proportional to frequency. However, on lower frequencies, the exact $1/f$ characteristic cannot be achieved. This is due to the fact that the filter described in (13) cannot approximate $1/\sqrt{f}$ accurately enough at low frequencies. The Allan variance of the noise is depicted in Fig. 2. It can be seen that at smaller time intervals, the Allan variance is approximately constant, which meets the expectation of the corresponding $\mu = 0$ value in Table I. On longer time intervals, the approximation becomes poor. This

can be explained since the approximation was poor at lower frequencies, and low frequencies correspond to high time interval values.

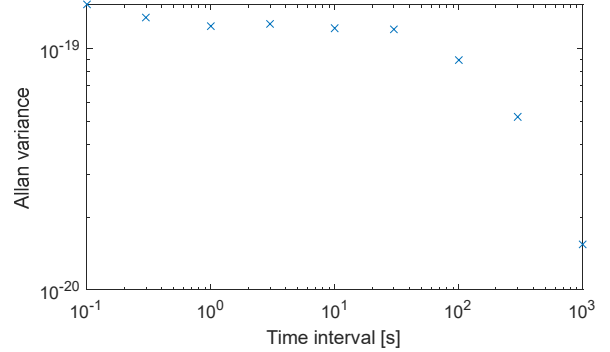


Fig. 2. Allan variance of the generated flicker frequency noise

As it has been demonstrated, flicker noise cannot be generated with arbitrary accuracy. To overcome this problem, two approaches can be applied. First, the order of the flicker filter defined in (13) can be increased. By this means, the approximation becomes better. The other approach is that the flicker noise is not generated in itself, but some noise source is also added that dominates flicker noise on long time intervals. In other words, a noise source is needed that has higher μ values, compared to flicker noise.

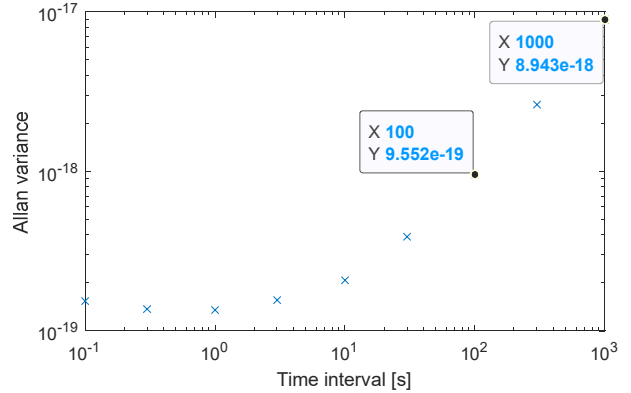


Fig. 3. Allan variance of the sum of flicker and random walk frequency noises

To this aim, let us generate flicker frequency noise, and add random walk frequency noise to it. The standard deviation of the white noise that is summed according to (11) is $\sigma_{WF^*} = 5 \cdot 10^{-11}$ s, while the standard deviation of the white noise that is filtered by (13) is $\sigma_{WF^{**}} = 10^{-8}$ s. The Allan variance of the sum of this two noise sources is depicted in Fig. 3. It can be seen that for short time intervals, the flicker noise dominates, resulting in an approximately constant Allan variance. If the time interval is increased, the random walk noise starts to dominate, and the Allan variance becomes proportional to the time interval, as it is determined by the $\mu = 1$ value of this noise source. Flicker phase noise can be generated in the same way, as flicker frequency noise. The only difference is that it influences values x_k instead of ϑ_k .

C. Noise due to temperature change

As it was mentioned in Section II.B, low-cost oscillators, and even TCXOs suffer from temperature-dependence. In the following, a TCXO will be considered that has a compensation algorithm for temperature dependence. However, this compensation is not perfect, and therefore the frequency is influenced by the temperature. Generally, in the datasheet of a TCXO, a maximum frequency error is provided along with a temperature range, within which this maximum error holds. Let us assume that the maximum relative error due to temperature change is

$$\vartheta_{TEMP,max} = 0.5 \text{ ppm} = 500 \text{ ppb} \quad (14)$$

in temperature range $[-50 \text{ }^\circ\text{C}; 80 \text{ }^\circ\text{C}]$. The error due to temperature dependence can be simulated in several ways. A possibility is that it is simulated to be a third-order polynomial:

$$\vartheta_{TEMP}(T) = k \cdot [a(T - T_0)^3 + b(T - T_0)^2 + c(T - T_0) + d], \quad (15)$$

where a , b , c , d and T_0 are random parameters and parameter k is needed to scale the polynomial so that it assumes its maximum value defined in (14). A result of such a polynomial generation is the following parameter set:

$$\begin{aligned} a &= 3.412 \\ b &= 4.058 \\ c &= -3.730 \\ d &= 4.134 \\ T_0 &= 6.618 \text{ }^\circ\text{C} \\ k &= 3.650 \cdot 10^{-13} \end{aligned} \quad (16)$$

The corresponding error function is depicted in Fig. 4. This temperature dependence is realistic, since it has small errors in the vicinity of $20 \text{ }^\circ\text{C}$, while the errors are increasing at the edges of the temperature range.

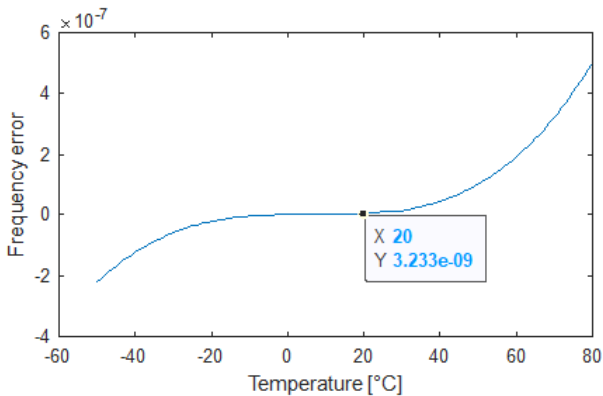


Fig. 4. Simulated frequency error of a TCXO as a function of temperature

In the following, three temperature profiles, and their effect on the frequency of the oscillator will be investigated. In the first case, it will be assumed that the oscillator is working at a constant temperature of $25 \text{ }^\circ\text{C}$. In the second case, an air-

conditioning profile will be applied. It will be assumed that when the temperature of the room reaches $26 \text{ }^\circ\text{C}$, air-conditioning is turned on. It cools the room down, and when $24 \text{ }^\circ\text{C}$ is reached, the air conditioning is turned off. Consequently, the room temperature will be increasing again, and so on. The result will be a triangle signal. The third profile will be simulating a case when a larger temperature change occurs, and the temperature increases in an exponential manner. It may occur when in an outdoor environment, sunshine increases the ambient temperature of the oscillator. This temperature profile will increase from $50 \text{ }^\circ\text{C}$ to $60 \text{ }^\circ\text{C}$.

The triangle and the exponential profile is depicted in Fig. 5. In both cases, three hours were simulated with a sampling frequency $f_s = 10 \text{ Hz}$. In the triangle profile, the room temperature was increasing for 25 minutes, and it was cooled for 5 minutes, and this pattern was repeated. In the exponential profile, the time constant of the increase was 15 minutes.

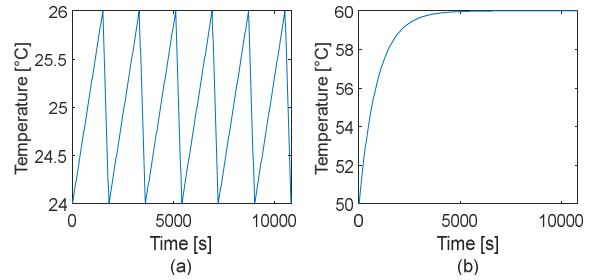


Fig. 5. Simulated temperature profiles: triangle (a) and exponential (b)

IV. THE EFFECT OF NOISE SOURCES

In this section, the effect of different noise sources on the Allan variance will be investigated. The effect of temperature-independent noise sources on the Allan variance is well-known, see Table I. These results will be used to validate the output of the noise generator of the model. Notwithstanding, the effect of temperature will be emphasized.

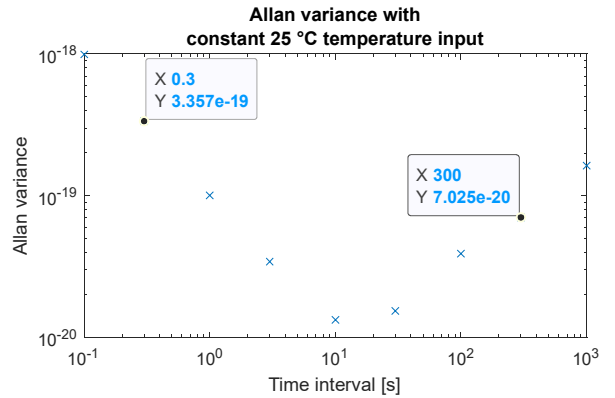


Fig. 6. Allan variance with a constant temperature profile

A. White and random walk frequency noise

In the following, the effect of white and random walk frequency noises will be considered. First, in order to check, whether the noise generation is correct, the constant temperature profile will be applied. The results are depicted in Fig. 6. If temperature dependence is also simulated, the Allan variance

values are plotted in Fig. 7. Results show that on short time intervals, temperature dependence only slightly modifies the Allan variance values.

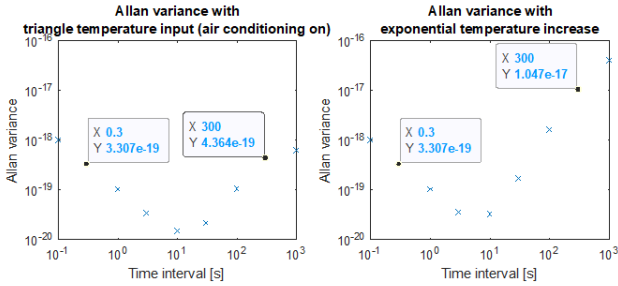


Fig. 7. Allan variance with triangle and exponential temperature profiles

Contrarily, for longer time intervals, differences become visible. This can be explained by the fact that temperature change occurs much slower than sampling. Therefore, samples that are close to each other are only slightly affected by temperature dependence, while longer time intervals imply higher temperature dependence. For the triangle pattern, the temperature varies between 24 °C and 26 °C. Fig. 4. shows that in this temperature interval, the frequency error characteristic of the simulated oscillator is flat. However, a more detailed analysis reveals that the errors are significantly different:

$$\begin{aligned} \vartheta_{TEMP}(24\text{ }^{\circ}\text{C}) &= 6.97\text{ ppb}, \\ \vartheta_{TEMP}(25\text{ }^{\circ}\text{C}) &= 8.21\text{ ppb}, \\ \vartheta_{TEMP}(26\text{ }^{\circ}\text{C}) &= 9.60\text{ ppb}. \end{aligned} \quad (17)$$

The result is that the slope of the Allan variance at longer time intervals increases. The same holds for the exponential temperature excitation, where the covered temperature range, and therefore the effect on the Allan variance is even larger.

A more detailed analysis of the Allan variance plots shows that $\mu \approx 1.3$ for the triangle pattern and $\mu \approx 1.5$ for the exponential pattern. However, it should be mentioned that for the triangle pattern, at 1000 seconds, the slope is decreased significantly. This is a topic for further investigations.

V. CONCLUSIONS

In this paper, an oscillator model for clock synchronization protocols has been introduced. Besides well-known Gaussian-type noise sources, also flicker noise has been generated, mentioning that it can only be supplied with finite precision. Nevertheless, this precision can be increased by increasing the order of the applied infinite impulse response filter. Furthermore, a model for the temperature dependence of the oscillator has been introduced. In the paper, a third-order frequency error model was considered, but any desired temperature dependence could be regarded during simulations. Since the effect of stationary noise sources is well-documented, the effect of temperature dependence on the Allan variance was emphasized. To this aim, three different temperature patterns have been generated. Firstly, the temperature was kept constant in order to have a reference Allan variance plot. Then,

triangular and exponential patterns have been generated in order to simulate the effect of air conditioning and exponential heating. Results show that the latter two temperature patterns affect the Allan variance for longer time intervals significantly. By adding temperature dependence as model input, a more realistic oscillator model was achieved that can also model different types of frequency and phase errors.

ACKNOWLEDGMENT

The research reported in this paper has been supported by the National Research, Development and Innovation Fund (TUDFO/51757/2019-ITM, Thematic Excellence Program), by the BME- Artificial Intelligence FIKP grant of EMMI (BME FIKP-MI/SC) and by Ericsson Magyarország Kft.

REFERENCES

- [1] D. Fontanelli, D. Macii, "Accurate time synchronization in PTP-based industrial networks with long linear paths", 2010 IEEE International Symposium on Precision Clock Synchronization for Measurement, Control and Communication, Portsmouth, NH, USA, Sept 27 – Oct. 1, 2010
- [2] X. Xu, Z. Xiong, J. Wu, X. Zhu, "High-precision time synchronization in real-time Ethernet-based CNC systems", *The International Journal of Advanced Manufacturing Technology*, vol. 65, no. 5-8, pp. 1157-1170, 2013
- [3] P. Ferrari, E. Sisinni, A. Flammini, A. Depari, Ferrari, Paolo, Emiliano Sisinni, Alessandra Flammini, and Alessandro Depari. "Adding accurate timestamping capability to wireless networks for smart grids", *Computer Networks*, vol. 67, pp. 1-13, 2014
- [4] *Precision Clock Synchronization Protocol for Networked Measurement and Control Systems*, IEC 61588:2009 – IEEE Standard 1588, 2008
- [5] *IEEE Standard Profile for Use of IEEE 1588™ Precision Time Protocol in Power System Applications*, IEEE Standard C37.238, 2017
- [6] X. Chen, D. Li, S. Wang, H. Tang, C. Liu, "Frequency-Tracking Clock Servo for Time Synchronization in Networked Motion Control Systems", *IEEE Access*, vol. 5, pp. 11606-11614, 2017
- [7] G. Giorgi, C. Narduzzi, "Performance Analysis of Kalman-Filter-Based Clock Synchronization in IEEE 1588 Networks", *IEEE Trans. Instrum. Meas.*, vol. 60, no. 8, pp. 2902-2909, 2011
- [8] Z. Fan, Y. Liu, H. Li, D. Yuan, H. Hu, "A servo design for slave clock in IEEE 1588 synchronization networks", *Int. J. Commun. Syst.*, vol. 28, pp. 615-624, 2015
- [9] C. Seong, S. Lee, W. Choi, "A New Network Synchronizer Using Phase Adjuster and Feedforward Filtering Based on Low-Cost Crystal Oscillators", *IEEE Trans. Instrum. Meas.*, vol. 59, no. 7, pp. 1764-1774., 2010
- [10] X. Xu, Z. Xiong, X. Sheng, J. Wu, X. Zhu, "A New Time Synchronization Method for Reducing Quantization Error Accumulation Over Real-Time Networks: Theory and Experiments", *IEEE Trans. Ind. Inf.*, vol. 9, no. 3, pp. 1659-1669, 2013
- [11] D. W. Allan, "Time and frequency (time-domain) characterization, estimation, and prediction of precision clocks and oscillators," *IEEE Trans. Ultrason., Ferroelect., Freq. Contr.*, vol. 34, no. 6, pp. 647–654, 1987.
- [12] J. Barnes, A. Chi, L. Cutler, D. Healey, D. Leeson, T. McGunigal, J. Mullen, W. Smith, R. Sydnor, R. Vessot, G. Winkler, "Characterization of Frequency Stability", *IEEE Trans. Instrum. Meas.*, vol. 20, no. 2, pp. 105-120, 1971
- [13] R. Vessot, L. Mueller, J. Vanier, "The specification of oscillator characteristics from measurements made in the frequency domain", *Proceedings of the IEEE*, vol. 54, no. 2, pp. 199-207, 1966
- [14] G. Gaderer, A. Nagy, P. Loschmidt, T. Sauter, "Achieving a Realistic Notion of Time in Discrete Event Simulation", *International Journal of Distributed Sensor Networks*, p. 11, Jan, 2011
- [15] J. S. Smith, "Spectral Audio Signal Processing", *W3K Publishing*, 2011